Numerical Simulation of the Gas-Liquid Flow in a Square Cross-sectioned Bubble Column *

N.G. Deen, T. Solberg and B.H. Hjertager
Chem. Eng. Lab., Aalborg Univ. Esbjerg, Niels Bohrs Vej 8, DK-6700 Esbjerg;
Tel. +45 7912 7610, Fax +45 7912 7677, Email: nd@aue.auc.dk,
URL: http://hugin.aue.auc.dk/

Summary

Bubble columns are widely used in the chemical and biochemical process industry. In order to develop design tools for engineering purposes, a large amount of research has been carried out in the area of CFD of gas-liquid flows. Amongst others, Becker et al. (Chem. Eng. Sci., vol. 49, p. 5747-5762, 1994) found that the gas-liquid flow in bubble columns shows pseudo-periodic behaviour. Sokolichin and Eigenberger (Chem. Eng. Sci., vol. 54, p. 2273-2284, 1999) used the k-ε model and 3D transient simulations to simulate the gas-liquid flow in 2D flat and 3D cylindrical bubble columns. Using this method, they found a grid independent pseudo-periodic solution. In the present paper the commercial code CFX 4.3 is used to simulate the gas-liquid flow in 3D rectangular bubble columns. Both these codes are 3D transient, and based on the two-fluid model. The turbulence viscosity in the liquid phase is modelled by the k-ε model and an expression, which takes the bubble-induced turbulence into account. The results of the simulations are compared with PIV and LDA measurements.

The simulations of the flow of a bubble plume in a flat bubble column correspond well with both the experiments and simulation results obtained by other researchers. Both the velocity and the velocity fluctuations are in quantitative agreement with experiments.

The movement of a bubble plume in a 3D bubble column was also simulated. In contrary to the other case only little temporal behaviour was found. This disagrees with the strongly time dependent flow, which was observed experimentally. In the simulation the bubble plume moves into one corner and stays there for the rest of the simulation time. This resulted in asymmetric velocity profiles. The velocity profiles are better predicted higher up in the column.

* To be presented at:
CHISA 14th Int. Congress of Chemical and Process Engineering, Praha, Czech Republic, August 27-31, 2000.

1. Introduction

Multiphase flows are widely used in the chemical and biochemical processindustry. Hydrodynamics often play an important role in these flows, therefore experimental and computational fluid dynamics (EFD and CFD) of multiphase flows have been a major topic in research and development since the 1970s. Much effort has been made to describe the flow phenomena in bubble columns. More recently attention has been focused on the dynamic behaviour of bubble columns. An overview of recent bubble column measurements, characterised by aspect ratio, superficial gas velocity and placement of the gas inlet is given in Table 1.

Table 1.
Parameters in experimental studies

Case	Reference	L/D	D/W	w_G (mm s^{-1})	Gas inlet
a.	Becker et al. (1994)	3	6.25	3.3	Left
b.	Becker et al. (1994)	3	6.25	0.66	Left
c.	Borchers et al. (1999)	1	6.25	0.41	Centre
d.	Borchers et al. (1999)	2	6.25	0.41	Centre
e.	Borchers et al. (1999)	3	6.25	0.41	Centre
f.	Borchers et al. (1999)	1	6.25	0.82	Centre
g.	Becker et al. (1999)	2.25	5	1.7	Centre
h.	Deen et al. (2000)	3	1	5.0	Centre

Becker et al. (1994) measured the flow pattern with laser doppler anemometry (LDA) in the case of a decentralized gas inlet, for a number of different aspect ratios and gas flow rates. Photographs of the bubble flow were taken, in order to make a qualitative interpretation of the gas hold-up. At low gas rates (i.e. case b.) they observed that the lower part of the bubble plume was stationary and directed to the left wall, under influence of a large liquid vortex on the right hand side. The upper part of the bubble plume was meandering in a quasi-periodic way. The period of this oscillating movement was found to be about 41 s. For higher gas rates (case a.) the meandering behaviour was not observed.

Borchers et al. (1999) focused on flows with a central gas inlet. They varied the aspect ratio of the columns. They observed a mainly stationary state for aspect ratios smaller than 1.5 (i.e. case c.). In that case one major circulation cell fills the entire diameter of the column. For larger aspect ratios a periodically meandering bubble plume was observed. Large vortices are moving down in the liquid next to the bubble plume. The period of the bubble plume movement turned out to be about 34 s. Chen et al. (1989) made streak photos of the flow in a flat bubble column at a gas superficial velocity of 35 mm s^{-1}. For different aspect ratios they observed a pattern of staggered vortices which corresponds well with the observations of Borchers et al. (1999).

Becker et al. (1999) performed measurements in a system comparable to that of Borchers et al. (1999) (i.e. case g). The main difference is that the column has other dimensions. The aspect ratio, L/D is larger than 1.5 and they observed a meandering bubble plume, which is in correspondence with the observations of Borchers et al. (1999). Becker et al. (1999) observed an oscillation period of about 17 s. They noted that the use of another sparger can reduce the oscillation period by 2 s.

Experiments of the flow of a bubble plume in a 3-D bubble column were performed by Deen et al. (2000) (case h). These experiments comprise a central plume rising in a column with an aspect ratio of 3. A meandering plume was observed. However, in contrary to the plumes in the flat bubble columns, which moved in a quasi-periodic fashion, the bubble plume in the 3-D column seems to be moving randomly. It was also observed that the presence of bubbles

introduces large turbulent fluctuations in the liquid phase. The measured slip velocity between the gas and the liquid phase was in the order of 0.2 m s^{-1}.

In this work the governing equations will be presented first. The interpretation of these equations by several authors for the simulation of bubble columns will then be discussed. The conclusions of this discussion will be used to set up simulations of the flow of a bubble plume in two bubble columns: a flat bubble column (i.e. the Becker case, case b) and a 3-D column (i.e. case h). The commercial code CFX 4.3 will be used for this purpose.

2. Theoretical background

2.1 Governing equations

Numerical simulations of gas-liquid bubbly flows have been carried out by a number of researchers. There is a variety of methods to simulate flow problems numerically. In this section only a general overview of the used methods will be given. The interested reader is encouraged to read the excellent review by Jakobsen et al. (1997) for information on these methods.
The continuity and momentum equations for the liquid phase are generally written as:

$$\frac{\partial(\alpha_L \rho_L)}{\partial t} + \nabla \cdot (\alpha_L \rho_L \mathbf{u}_L) = 0 \tag{2.1}$$

$$\frac{\partial(\alpha_L \rho_L \mathbf{u}_L)}{\partial t} + \nabla \cdot (\alpha_L \rho_L \mathbf{u}_L \mathbf{u}_L) = -\nabla \cdot (\alpha_L \tau_L) - \alpha_L \nabla P + \alpha_L \rho_L \mathbf{g} + \mathbf{M}_I \tag{2.2}$$

with τ_L the stress tensor:

$$\tau_L = -\mu_{eff,L}\left(\nabla \mathbf{u}_L + (\nabla \mathbf{u}_L)^T - \tfrac{2}{3}\mathbf{I}(\nabla \cdot \mathbf{u}_L)\right) \tag{2.3}$$

where $\mu_{eff,L}$ is the effective viscosity, which is composed of three contributions; the molecular viscosity, the turbulent viscosity and an extra term due to bubble induced turbulence:

$$\mu_{eff,L} = \mu_{l,L} + \mu_{t,L} + \mu_{BI,L} \tag{2.4}$$

The turbulent viscosity is based on the k-ε model and formulated as follows:

$$\mu_{t,L} = \rho_L C_\mu \frac{k^2}{\varepsilon} \tag{2.5}$$

The turbulent kinetic energy k and the energy dissipation ε are calculated from their conservation equations:

$$\frac{\partial(\alpha_L \rho_L k)}{\partial t} + \nabla \cdot (\alpha_L \rho_L \mathbf{u}_L k) = -\nabla \cdot (\alpha_L \frac{\mu_{t,L}}{\sigma_k} \nabla k) + \alpha_L (G - \rho_L \varepsilon) \tag{2.6}$$

$$\frac{\partial(\alpha_L \rho_L \varepsilon)}{\partial t} + \nabla \cdot (\alpha_L \rho_L \mathbf{u}_L \varepsilon) = -\nabla \cdot (\alpha_L \frac{\mu_{t,L}}{\sigma_{T,\varepsilon}} \nabla \varepsilon) + \alpha_L (C_{\varepsilon 1} \frac{\varepsilon}{k} G - C_{\varepsilon 2} \rho_L \frac{\varepsilon^2}{k}) \tag{2.7}$$

with the following model constants $C_\mu = 0.09$; $\sigma_k = 1.00$; $\sigma_\varepsilon = 1.30$; $C_{\varepsilon 1} = 1.44$ and $C_{\varepsilon 2} = 1.92$. The term G in Eqs. (2.6) and (2.7) is the production of turbulent kinetic energy and described as:

$$G = \tau_L : \nabla \mathbf{u}_L \tag{2.8}$$

There are several models available to take account of the turbulence induced by the movement of the bubbles. In this study the model proposed by Sato (1975) was used:

$$\mu_{BI,L} = \rho_L C_{\mu,BI} \alpha_G d_B \left| \mathbf{u}_G - \mathbf{u}_L \right| \tag{2.9}$$

with $C_{\mu,BI}$ a model constant which equals 0.6.

In the Lagrangian approach the movement of bubbles in a gas-liquid flow is modelled with the use of a force balance for every bubble:

$$\frac{D(\rho_G V_b \mathbf{u}_g)}{Dt} = -V_b \nabla P + \rho_G V_b \mathbf{g} - \mathbf{m}_I \tag{2.10}$$

with $\mathbf{m}_I$ the momentum transfer at the bubble interface, which will be defined later. In the Lagrangian approach each bubble is tracked individually, i.e. a force balance is solved for every bubble in the system. In the Eulerian approach bubbles are no longer tracked individually, but the ensemble average, (i.e. the local gas hold-up, α_G) is used:

$$\alpha_G = n V_b \tag{2.11}$$

When Eq. (2.10) is summed over all n bubbles and Eq. (2.2) is substituted, the Eulerian momentum equation for the gas phase is found:

$$\frac{\partial(\alpha_G \rho_G \mathbf{u}_g)}{\partial t} + \nabla \cdot (\alpha_G \rho_G \mathbf{u}_g \mathbf{u}_g) = -\alpha_G \nabla P + \alpha_G \rho_G \mathbf{g} - \mathbf{M}_I \tag{2.12}$$

An additional stress term can be included in Eq. (2.12). This term should not be interpreted as a diffusion term, since the bubbles can be regarded as solid, and thus non-diffusive, entities. In stead this stress term represents the dispersion of bubbles in the liquid:

$$\frac{\partial(\alpha_G \rho_G \mathbf{u}_g)}{\partial t} + \nabla \cdot (\alpha_G \rho_G \mathbf{u}_g \mathbf{u}_g) = -\nabla \cdot (\alpha_G \tau_G) - \alpha_G \nabla P + \alpha_G \rho_G \mathbf{g} - \mathbf{M}_I \tag{2.13}$$

Nevertheless, the dispersion term has the same form as the diffusion term in the momentum equation for the liquid phase. The calculation of the effective gas viscosity is based on the effective liquid viscosity as follows:

$$\mu_{eff,G} = \frac{\rho_G}{\rho_L} \mu_{eff,L} \tag{2.14}$$

as was proposed by Jakobsen et al. (1997) and also used by Friberg (1998).
In the Eulerian approach an additional continuity equation is needed for the gas phase:

$$\frac{\partial(\alpha_G \rho_G)}{\partial t} + \nabla \cdot (\alpha_G \rho_G \mathbf{u}_G) = 0 \qquad (2.15)$$

No mass transfer between the phases is assumed (i.e. the right hand sides in equations 2.1 and 2.15 are zero). The continuity and momentum equations for liquid and gas (Eqs. 2.1, 2.2, 2.13 and 2.15), together with the two equations for the k-ε model (Eqs. 2.6 and 2.7) form the total set of differential equations that describe the system. These equations will be used in this work.

The interfacial momentum transport between both phases is expressed in the term $\mathbf{M}_I$. This term can consist of several forces, like for example the drag, lift, virtual mass, lubrication and wall forces (i.e. see Jakobsen et al. (1997)). These forces are normally described with analytical models, which contain empirical constants. The drag force is the most important force and is described as follows:

$$M_{D,i} = -\tfrac{3}{4}\alpha_G \alpha_L \rho_L \frac{C_D}{d_b} |\mathbf{u}_G - \mathbf{u}_L| (u_{G,i} - u_{L,i}) \qquad (2.16)$$

The drag coefficient C_D is dependent on the bubble Reynolds number, Re_b. Tomiyama (1998) proposed the following equation for flow of bubble flow in slightly contaminated water:

$$C_D = \max\left[\min\left[\frac{24}{\mathrm{Re}_b}(1 + 0.15\,\mathrm{Re}_b^{\,0.687}), \frac{72}{\mathrm{Re}_b} \right], \frac{8}{3}\frac{\mathrm{Eo}}{\mathrm{Eo}+4} \right] \qquad (2.17)$$

Where Eo the Eötvös number. Another drag relation proposed by Ishii and Zuber given by:

$$C_D = \tfrac{2}{3}\mathrm{Eo}^{\frac{1}{2}} \qquad (2.18)$$

Note that Eq. (2.18) should be corrected for higher gas hold-ups (i.e. see for example Hjertager (1998)). This is not done in this work, since the gas hold-up is rather low.
At a typical bubble size of 4 mm and a relative velocity of 0.2 m s^{-1} the drag coefficient in Eq. (2.17) will be based on the Eötvös number. In that case, the resulting drag coefficients for both equations are very similar, i.e C_D = 1.63 for Eq. (2.17) and C_D = 1.67 for Eq. (2.18). In this work the Eq. (2.18) will be used.

Depending on the physical problem (i.e. flow regime, gas holdup, etc.) other interface forces play a more or less important role. The choice of a coefficient for the lift force is strongly problem dependent and will therefore not be discussed here. The virtual mass force turns out to be only of importance in the case of strong accelerations, which mainly occur in the surrounding of the gas inlet. For a detailed discription and a discussion of the form of the interface forces the reader is referred to the work of Delnoij et al. (1997), Jakobsen et al. (1997), Hjertager (1998) and Friberg (1998).

2.2 Previous work

A brief overview of the methods of other authors is given in Table 2.

Table 2.
Parameters in numerical studies. E-E is Euler-Euler, E-L is Euler-Lagrange, D is drag force, VM is virtual mass force, L is lift force, BB is bubble-bubble collisions, TP is turbulent pressure force and TD is turbulent dispersion force.

Reference	Case	Model	Forces	2D/3D	Turb.	Diff. Scheme
Sokolichin and Eigenberger (1994)	a,b	E-E	D	2D	None	?
Becker et al. (1994)	a,b	E-E	D	2D	None	?
Sokolichin et al. (1997)	b	E-E/E-L	D	2D	None	TVD Upwind
Delnoij et al. (1997)	a,b	E-L	D, VM, L, BB	2D	None	Upwind
Sokolichin and Eigenberger (1999)	c-f	E-E	D	2D/3D	None/k-ε	TVD Upwind
Borchers et al. (1999)	c-f	E-E	D	3D	k-ε	TVD
Mudde and Simonin (1999)	b	E-E	D D, VM, TP	2D/3D	None/k-ε	? O(3)
Pfleger et al. (1999)	g	E-E	D D, TD	2D/3D	None/k-ε	TVD
This work	b,h	E-E	D	3D	k-ε	Quick

Sokolichin et al. (1997) compared the results of the Eulerian and Lagrangian approaches. They noticed that the Eulerian approach suffers from numerical diffusion. This is due to the fact that the gas fraction is smeared out over the entire grid cell, while in the Lagrangian approach the position of every bubble within the grid cell is recorded. In order to reduce numerical diffusion in the Eulerian approach, they suggested the use of higher order discretization order schemes, like the Total Variation Diminishing scheme (TVD). The main conclusion of their work was that when an appropriate discretization scheme is used, there are no substantial differences between the results of the two approaches. Sokolichin and Eigenberger (1999) illustrated this once more by comparing the results of their Eulerian model with TVD scheme, with the Lagrangian results of Delnoij et al. (1997), which were obtained with upwind discretization. They noticed that both methods gave similar results.

The laminar simulations of Becker case b showed only small discrepancies with respect to the dynamic behaviour of the bubble plume. Delnoij et al. (1997) found an oscillation period of about 30 s, which is 10 s shorter than the experimental findings. Becker et al. (1994), Delnoij et al. (1997) and Sokolichin and Eigenberger (1999) all noticed in their predictions that the lower part of the bubble plume was oscillating along with the rest of the plume. In the experiments however this behaviour was not observed. Sokolichin and Eigenberger (1999) found out that Becker et al. (1994) and Delnoij et al. (1997) made some "lucky shots", i.e. when the grid is refined completely other behaviour was found. In other words the solutions were grid dependent. It was thought that one of the sources of this problem was that the flow is not laminar as was assumed in the simulations. Therefore the use of a k-ε model was suggested. The k-ε model however introduces a much higher viscosity, which dampens out all the periodic behaviour in 2D simulations.

Mudde and Simonin (1999), Sokolichin and Eigenberger (1999), and Pfleger et al. (1999) showed that, in order to get a grid independent pseudo periodic solution employing a k-ε model, 3-dimensional simulations are required. In this case the effective viscosity gets a lower

value than in the 2D simulations. This makes the occurrence of large fluctuating motions possible.

Using 3D simulations and the k-ε model, Sokolichin and Eigenberger (1999) observed an oscillation period of about 40 s, which corresponds very well with the experimental findings. They used three different grids and observed that the time averaged results were basically the same for all grids. The only discrepancy left is the underestimation by a factor two of the liquid velocity close to the sparger. This might be due to the fact that the virtual mass force, which takes account of acceleration effects, was not modelled. Borchers et al. (1999) showed that the use of 3D turbulent simulations also gave good results for the cases c-f.

Pfleger et al. (1999) mentioned that bubble induced turbulence may play an important role. This can be modelled by introducing an extra term in the k-equation (see for example Friberg (1998)) or by using the model proposed by Sato (1975), which was mentioned earlier. In their paper however Pfleger et al. (1999) restricted themselves to the use of the standard k-ε model. They investigated the use of a turbulent dispersion term in the continuity equation of the gas phase, Eq. (2.14), instead. The use of turbulent dispersion slowed down the periodic behaviour. Pfleger et al. (1999) therefore concluded that the use of a turbulent dispersion term in the continuity equation is not necessary. It is important to realise that the use of schemes with less numerical diffusion or finer grids may still need turbulent dispersion terms though.

Mudde and Simonin (1999) obtained an oscillating solution with the use of 3D turbulent simulations. The oscillation period however was an order of magnitude too short. This problem was solved by incorporating the virtual mass force in the simulations. It should be noted that Mudde and Simonin (1999) incorporated turbulent dispersion of the gas phase in the momentum equations. This might be necessary, because the third order discretization scheme does not provide sufficient other diffusion (i.e. numerical diffusion).

3. Case studies

As mentioned earlier two test cases will be investigated. The first is the Becker case (i.e. case b.). The other case is based on the experiments described in Deen et al. (2000) (i.e. case h.). Both cases will be simulated with CFX 4.3. In this section a short description of the experimental set-up, the experimental procedures and the CFD implementation will be given.

3.1 Experiments

Becker et al. (1994) performed LDA measurements in a pseudo 2-D bubble column, filled with tap water. This flat bubble column was 0.5 m wide, 2 m high and 0.08 m deep. A gas sparger, positioned 0.15 m from the left wall, was used to introduce an air flow of 1.6 l min^{-1} into the system. The circular sparger had a diameter of 40 mm and a pore size of 40 μm.

Deen et al. (2000) performed measurements in a 3-D bubble column filled with distilled water. 4 g of kitchen salt per litre water was used in order to obtain a non-coalescing system. The column has a square cross-section (WxD) of 0.15 x 0.15 m^2 and a height (L) of 1 m. Air was introduced into the system through a perforated plate. The plate contained 49 holes, with a diameter of 1 mm, which were positioned in the middle of the column at a square pitch of 6.25 mm. A particle image velocimetry (PIV) system combined with laser-induced fluorescence (LIF) was used to simultaneously measure the gas and liquid velocities. In addition, an LDA system was used to measure the liquid velocity.

3.2 Spatial and temporal resolution

Both geometries were modelled using cubic grid cells of 1 cm^3. For case b this corresponds to 8 x 50 x 160 (w x d x l) = 64,000 cells. For case h this results in 15 x 15 x 50 = 11,250 cells. The timestep is set to a fixed value of 0.01 s. For typical values of the maximum velocity 0.5 m s^{-1} and minimum gridsize of 0.01 m, one can expect a Courant number in the order of 0.5.

To prevent the column from flooding, ten extra cells were used at the top of the column for case b. In case h. five extra cells were used.

3.3 Boundary conditions

The boundary conditions were defined at the inlet as follows:

$$v_{G,in} = \frac{w_G WD}{\alpha_G A_{in}} \tag{3.1}$$

with w_G the superficial gas velocity and WxD the cross sectional area of the column
In the Becker case the circular inlet is approximated with a square gas inlet of 4x4 gridcells (i.e. 4x4 cm^2). For a superficial gas velocity of 0.66 mm s^{-1} and a gas volume fraction of 1.0 the gas velocity at the inlet becomes 0.0167 m s^{-1}.

In test case h the gas inlet was implemented in a central area of 3x3 gridcells (i.e. 3x3 cm^2). In this case for a superficial gas velocity of 5 mm s^{-1} a gas velocity at the inlet of 0.125 m s^{-1} is calculated.

The law of the wall was used to set the boundary conditions for the liquid phase at the wall. A no-slip condition was used for the gas phase at the wall.

At the outlet a pressure boundary was used in the CFX simulations. In the Flotracs simulation the liquid velocities were set to zero at the outlet, while the gas velocities were determined from the gas inflow.

3.4 Differencing scheme

In the simulations, a bounded third order accurate QUICK scheme was used for the discretization of the convection terms. This is a differencing scheme that resembles the TVD scheme.

4. Results

4.1 2D bubble column

The Becker case b (i.e. see Table 1.) has been modelled as described in the previous section with the use of CFX 4.3. Eight snapshots of the volume fraction of the gas phase are displayed in Fig. 1. An oscillating behaviour can clearly be observed. This qualitative behaviour is in close agreement with the results of Mudde and Simonin (1999) and Sokolichin and Eigenberger (1999). There is a small discrepancy between the simulation and the experiment in the bottom left side of the column. In this side, the bubble plume is occasionally pushed rightwards, as can be seen in the fifth snapshot in Fig. 1. This behaviour was not observed by Becker et al. (1994).

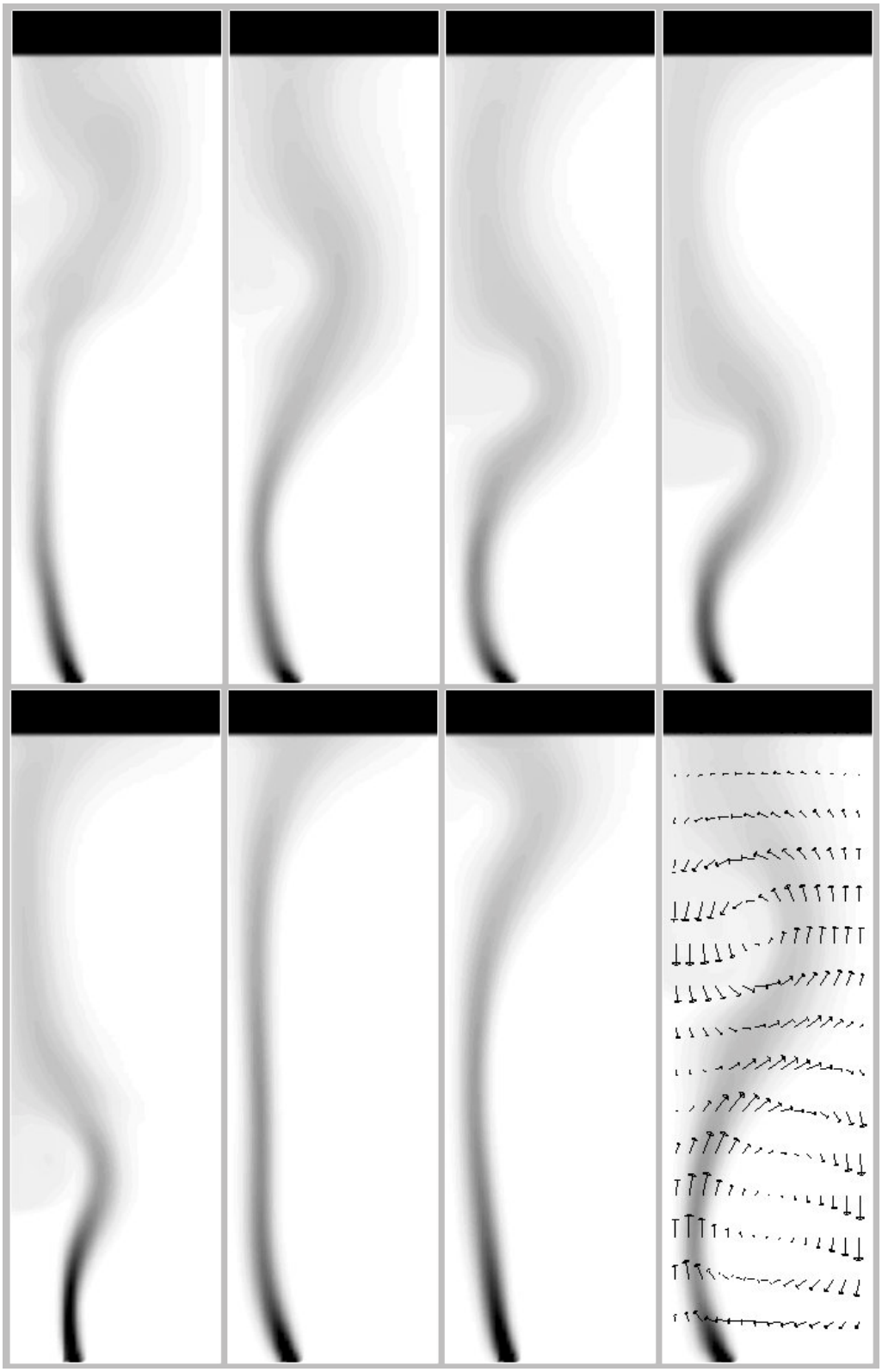

Fig. 1. Plots of the volume fraction of the gas phase, ε_G at eight different instances, with time intervals of 10 s. White corresponds to $\varepsilon_G = 0$ and black to $\varepsilon_G > 0.05$. The last plot also shows the velocity field of the liquid phase.

In Fig. 2, the axial liquid velocity as a function of time is displayed. The velocity is recorded at the point x = 0.035 m, y = 0.040 m, z = 0.900 m. This corresponds to one of the monitoring points used by Becker et al. (1994), so a direct comparison can be made. In correspondence with the experiment, the simulated plume oscillation is observed to be pseudo-periodic. As in

the experiment, the simulated trend differs from period to period. The simulated oscillation period is in the order of 60 s. This is 20 s longer than the oscillation period of 40 s observed by Becker et al. (1994). What is causing this difference is not quite clear. Eigenberger and Sokolichin (1997) found oscillation periods between 40 and 60 s, depending on the grid size. Becker et al. (1999) indicated that the sparger design influenced the oscillation period. Differences in the numerical and the experimental sparger design may therefore explain the differences in oscillation time.

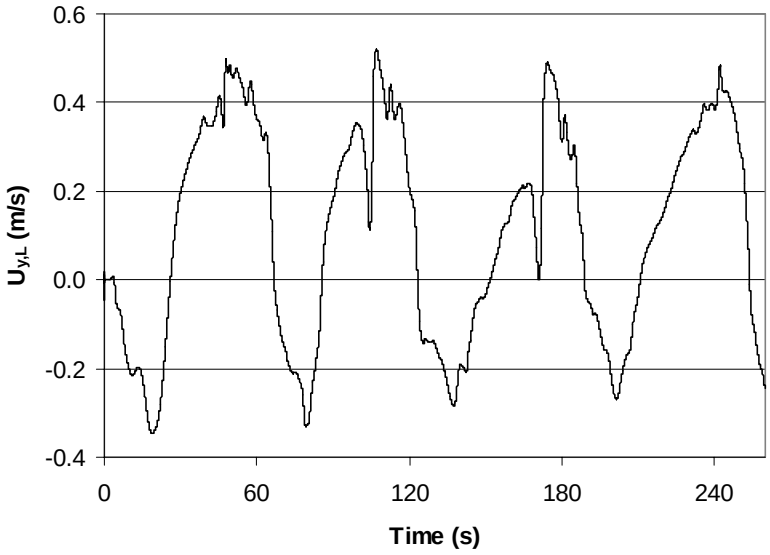

Fig 2. Time plot of the axial velocity component of the liquid phase at one point in the bubble plume, x = 0.035 m, y = 0.040 m, z = 0.900 m.

In Fig. 3, the simulation results are compared with the experiments more quantitatively. This figure shows time-averaged profiles of the axial liquid velocity at a height of 0.800 m. It can be seen that there is a good agreement between the measured and the simulated profiles.

The time-averaged fluctuations in the liquid velocity are displayed in Fig. 4. These have been determined as follows:

$$\overline{u}_i = \frac{1}{N}\sum_{k=1}^{N} u_i(k) \tag{4.1}$$

$$\overline{u}_{i,rms} = \frac{1}{N}\sum_{k=1}^{N} (u_i(k) - \overline{u}_i)^2 \tag{4.2}$$

Both with respect to the trend as the order of magnitude the simulated fluctuations correspond rather well with the measurements of Becker et al. (1994). The maximum of the radial fluctuations at the centreline is due to the oscillation of the bubble plume. The large gradients in the axial velocity in the right side of the column result in a maximum of the axial velocity fluctuations in that area.

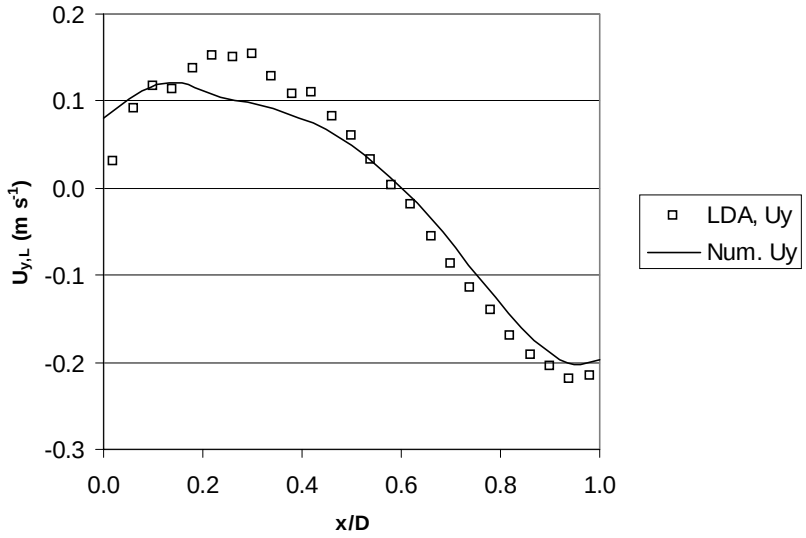

Fig. 3. Time averaged plot of the axial velocity component of the liquid phase at y = 0.040 m, z = 0.800 m. Experimental data by Becker et al. (1994).

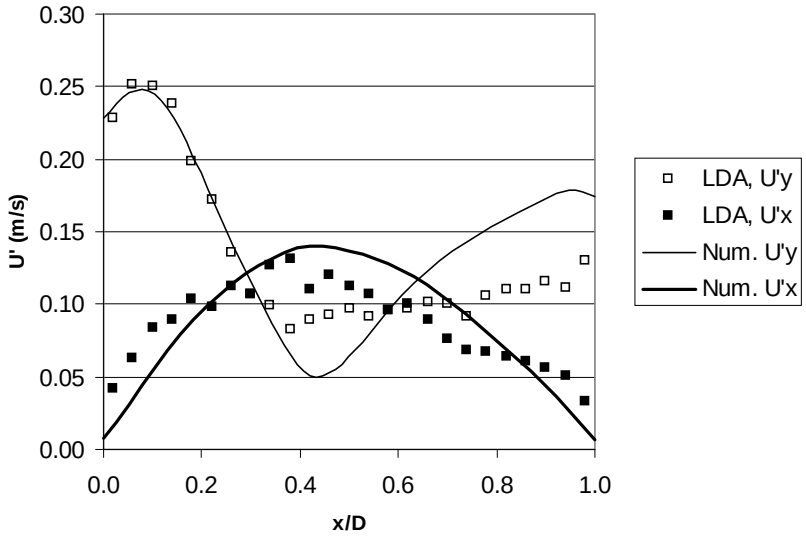

Fig. 4. Time averaged plot of the axial and radial velocity fluctuations of the liquid phase at y = 0.040 m, z = 0.800 m.

4.2 3D bubble column

The experimental case described by Deen et al. (2000) (i.e. case h) has also been modelled with the use of CFX 4.3. Three arbitrary snapshots of the iso-surface of a gas phase volume fraction of 10% are displayed in Fig. 5. At the bottom of the column, the bubble plume swings towards one corner, under influence of a strong liquid vortex at the right side of the column. Higher in the column the orientation of the plume is changed toward the centre line of the column again. Secondary weaker vortices occur just underneath the liquid surface on both sides of the column. These vortices are not strong enough to push the bubble plume out of its corner. As a result, the three snapshots look very much alike. These observations do not agree with the experimental observations of Deen et al. (2000) which showed a bubble plume moving randomly around the centre line.

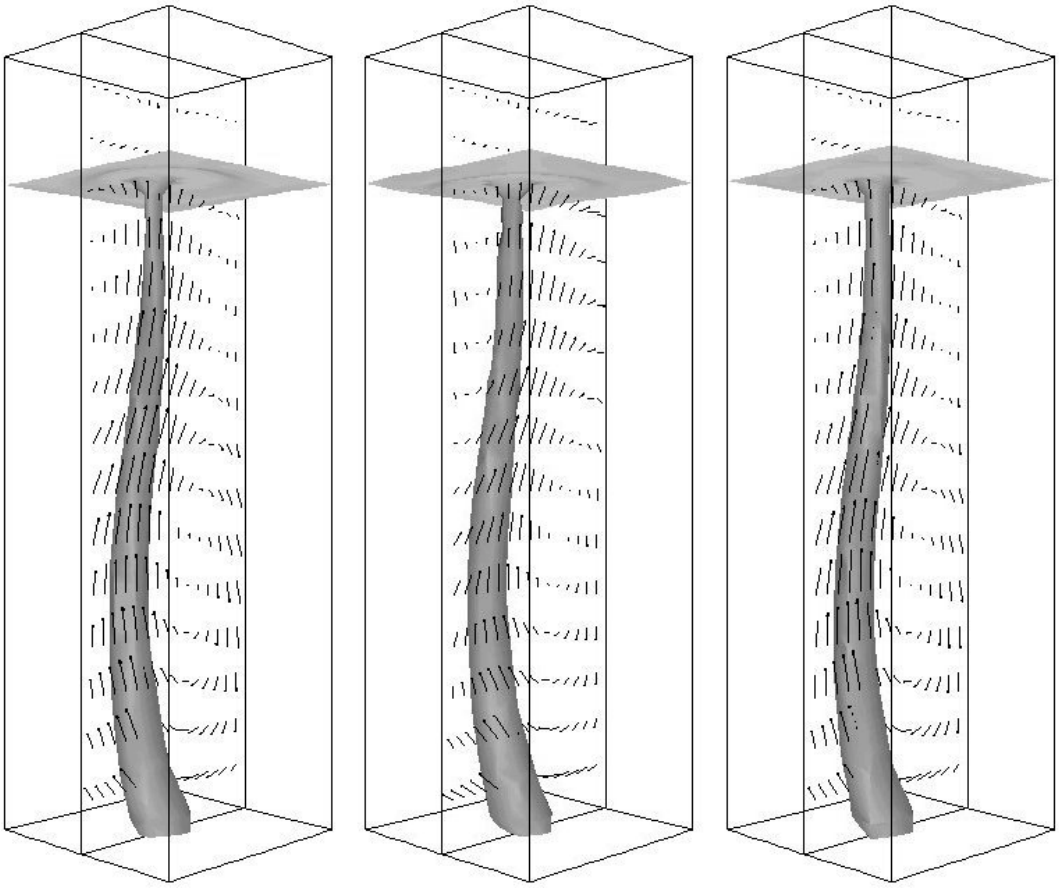

Fig. 5. Three snapshots of the iso-surface of the bubble plume in case h (i.e. the surface indicates $\varepsilon_G = 0.1$). The liquid velocity field in the centre plane is also shown. The plots are respectively 100, 200 and 300 s after the start of the simulation.

A better impression of the transient behaviour of the bubble plume can be obtained from Figs. 6 and 7. In these figures the axial and the radial liquid velocity components are monitored as a function of time. The simulation results are superimposed on LDA measurements performed in the same column as described by Deen et al. (2000). Since the LDA data contains a high level of scatter, a moving average with a sample size of 100 is calculated. From Fig. 6, the axial liquid velocity can be seen to fluctuate around 0.2 m s^{-1}. The high peak in the simulation around 0 s is due to the start-up of the column. As was to be expected, the turbulent fluctuations are not captured by the simulation. The large scale fluctuations however seem to be in the same order of magnitude as the fluctuations in the moving average.

The simulated radial velocity is oscillating between 0.03 m s^{-1} and 0.05 m s^{-1}, as can be seen in Fig. 7. This deviates from the experiments, which show an oscillation around zero. This is due to the fact that in the simulation the bubble plume is permanently positioned in one corner of the column. The oscillations in the simulation have a period of about 14 s. Figs. 6 and 7 clearly show that the simulation is time dependent. However the level of resolved fluctuations is rather low. One of the reasons might be that the k-ε model gives a structural overestimation of the viscosity in the liquid phase. This reduces the possibilities for small structures to form.

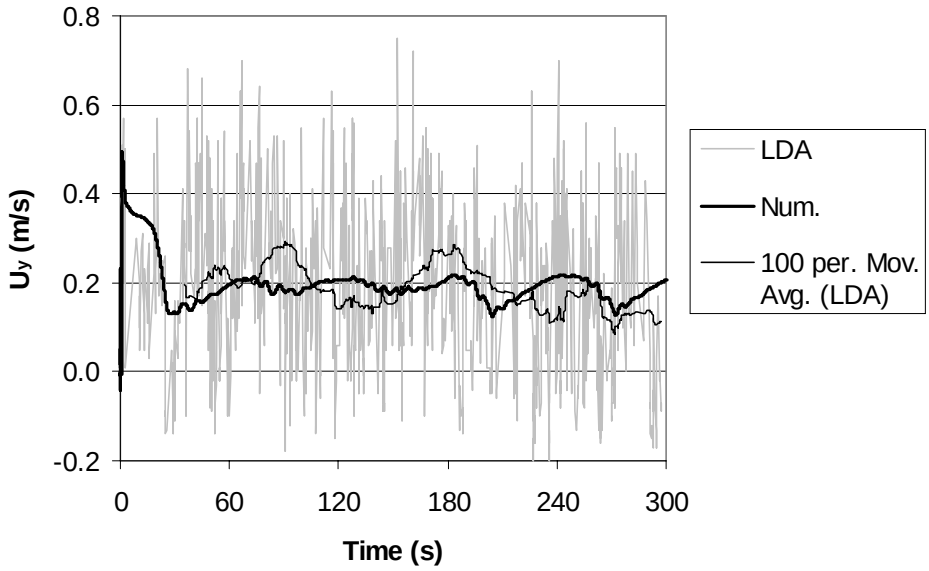

Fig. 6. Time plot of the axial velocity component of the liquid phase at a point on the centreline of the column, x = 0.075, y = 0.075, z = 0.250.

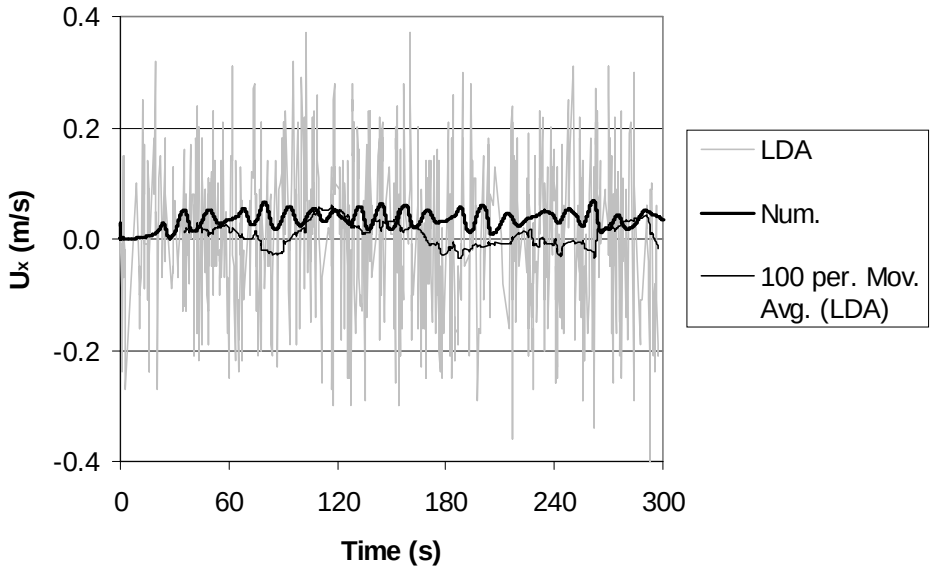

Fig. 7. Time plot of the radial velocity component of the liquid phase at a point on the centreline of the column, x = 0.075, y = 0.075, z = 0.250.

A quantitative comparison between the simulation results and the experiments is in Figs. 8 and 9. In these figures, time-averaged velocity profiles at three different heights are compared with PIV and LDA. Since the predicted bubble plume is confined into one corner, the velocity profiles for both phases at heights of 0.15 m and 0.25 m are non-symmetrical. This behaviour is not observed in the experimental data. The asymmetry leads to an overestimation of the velocities on the left side of the column and an underestimation on the right side. At a height of 0.35 m the simulated profile is more symmetric. At that height the simulated core annulus profiles of the liquid velocity correspond rather well with the experimental data. When the simulated asymmetry is taken into account, the simulated gas velocity is slightly overestimated at all heights.

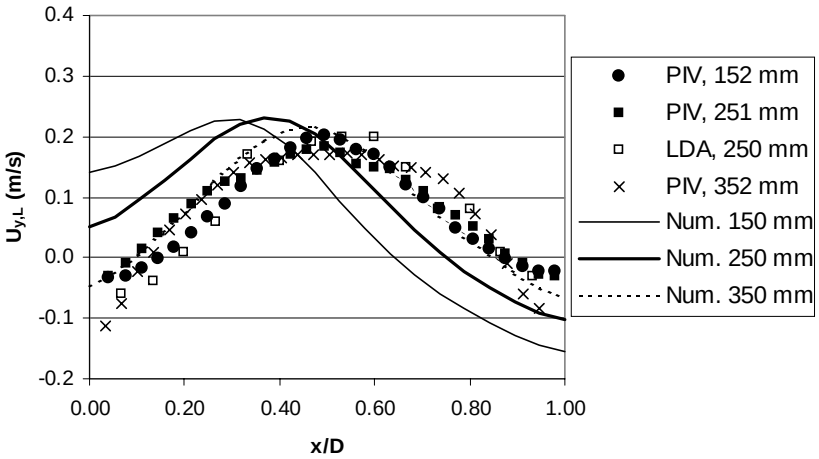

Fig. 8. Time averaged plot of the axial velocity component of the liquid phase at different heights in the column.

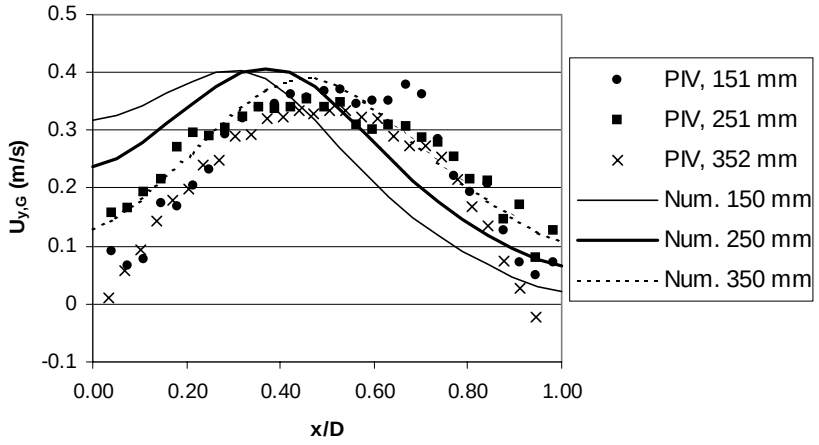

Fig. 9. Time averaged plot of the axial velocity component of the liquid phase at different heights in the column.

In Fig. 10, the time averaged turbulent kinetic energy in the liquid phase, k is compared with both PIV and LDA experiments. It should be noted that in the experiments isotropy in the radial direction is assumed and k is approximated accordingly as follows:

$$k = \tfrac{1}{2}\left(2\overline{u_x'^2} + \overline{u_y'^2}\right) \qquad (4.3)$$

Clearly there is a large difference between the values for k in the LDA and PIV data. The lower k values for the PIV can be due to the fact that the measured velocities are based on an ensemble average of the tracer particles within the measurement volume. This ensemble average will filter out some of the high frequency fluctuations. The PIV measurement data may therefore be systemetically underestimated.

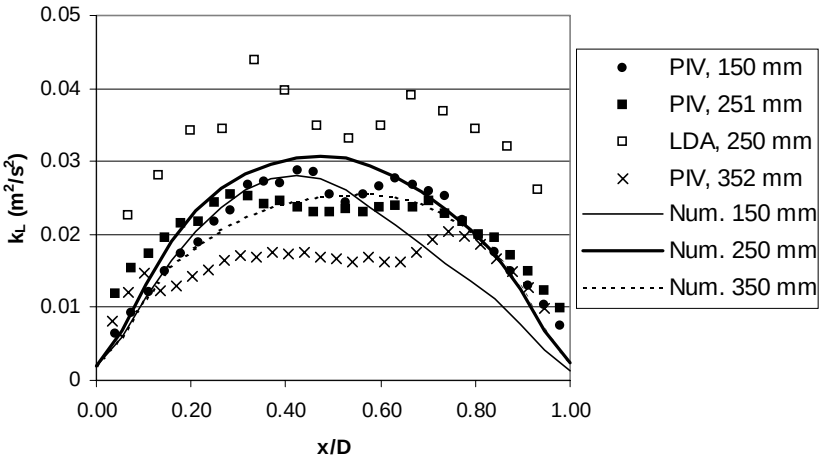

Fig. 10. Time averaged plot of the time averaged turbulent kinetic energy of the liquid phase at different heights in the column.

In all the measured profiles in Fig. 10 a local minimum of k can be observed close to the centreline. This is probably due to the oscillation of the bubble plume. That is, large vortices with high levels of turbulence are present next to the bubble plume. Since the bubble plume does not show these large scale oscillations, the local minimum is not observed. The simulated values for k at an height of 0.35 m are mostly positioned between the PIV and LDA data. Only near the walls the values for k are lower then both measured curves. At heights of 0.15 m and 0.25 m the order of magnitude of the turbulent kinetic energy is captured rather well. k is underestimated at a height of 0.15 m.

5. Conclusions

Numerical simulations of the flow of a bubble plume in two rectangular bubble columns have been presented. After a discussion of previous work, the flow was described with the two-fluid model, where only the drag force was taken into account. The simulations were performed in 3D and time-dependent. The turbulence viscosity in the liquid phase was modelled with the k-ε model. An extra contribution in the effective viscosity for the turbulence induced by bubbles was taken into account. The higher order QUICK scheme was used to discretize the convection terms in the equations.
The simulations of the flow of a bubble plume in a flat bubble column correspond well with both the experiments of Becker et al. (1994) and the simulation results obtained by Sokolichin and Eigenberger (1999). That is, a pseudo periodic movement of the bubble plume was observed. The largest difference between the simulations and experiments was the overestimation of the oscillation period by 20 s. Both the velocity and the velocity fluctuations are in quantitative agreement with the measurement data of Becker et al. (1994).
The movement of a bubble plume in a 3D bubble column was also simulated. In contrary to the other case only little temporal behaviour was found. This disagrees with the strongly time dependent flow observed by Deen et al. (2000). In the simulation the bubble plume moves into one corner and stays there for the rest of the simulation time. This resulted in asymmetric velocity profiles. The velocity profiles are predicted better higher up in the column.
The grid-dependency of the simulations and the modelling of the gas inlet have not been investigated. These points will need further attention in future research.

6. Symbols

A	Area (m^2)
C_μ	Model constant k-ε model (-)
$C_{\mu,BI}$	Model constant bubble induced turbulence (-)
$C_{\varepsilon 1}$	Model constant k-ε model (-)
$C_{\varepsilon 2}$	Model constant k-ε model (-)
C_D	Drag coefficient (-)
D	Column depth (m)
d_B	Bubble diameter (m)
$\mathbf{g}$	Gravitational constant ($m^2\ s^{-1}$)
G	Production of turbulent kinetic energy ($kg\ m^{-1}\ s^{-3}$)
$\mathbf{I}$	Unity tensor (-)
k	Turbulent kinetic energy ($m^2\ s^{-2}$)
L	Column height (m)
$M_{D,I}$	Eulerian drag force component in direction i (N)
$m_{D,I}$	Lagrangian drag force component in direction i (N)
$\mathbf{M}_I$	Eulerian interfacial force (N)
$\mathbf{m}_I$	Lagrangian interfacial force (N)
n	Bubble number concentration (m^{-3})
P	Pressure ($N\ m^{-2}$)
$\mathbf{u}$	Velocity vector ($m\ s^{-1}$)
u_i	Velocity component in direction i ($m\ s^{-1}$)
u_I'	Velocity fluctuation in direction i ($m\ s^{-1}$)
W	Column width (m)
w_G	Superficial gas velocity ($m\ s^{-1}$)

6.1 Greek symbols

α	Volume fraction (-)
ε	Energy dissipation ($m^2\ s^{-3}$)
ρ	Density ($kg\ m^{-3}$)
σ_k	Model constant k-ε model (-)
σ_ε	Model constant k-ε model (-)
σ	Surface tension ($N\ m^{-1}$)
τ	Stress tensor ($kg\ m^{-1}\ s^{-2}$)
μ_l	Kinematic viscosity ($m^2\ s^{-1}$)
μ_t	Turbulent viscosity ($m^2\ s^{-1}$)
μ_{eff}	Effective viscosity ($m^2\ s^{-1}$)

6.2 Subscripts

G	Gas phase
in	Inlet
L	Liquid phase

6.3 Dimensionless numbers

Re_b	Bubble Reynolds number = $\rho_L\ d_B\ u_{rel} / \mu_l$
Eo	Eötvös number = $g\Delta\rho\ d_B^2/\sigma$

7. References

Becker, S., De Bie, H. and Sweeney, J. (1999) Dynamic flow behaviour in bubble columns, *Chem. Eng. Sci., 54*, pp.4929-4935

Becker, S., Sokolichin, A. and Eigenberger, G. (1994) Gas-liquid flow in bubble columns and loop reactors: Part II. Comparison of detailed experiments and flow simulations, *Chem. Eng. Sci., 49*, pp.5747-5762

Borchers, O., Busch, C., Sokolichin, A. and Eigenberger, G. (1999) Applicability of the standard k-ε turbulence model to the dynamic simulation of bubble columns. Part II: Comparison of detailed experiments and flow simulations, *Chem. Eng. Sci., 54*, pp.5927-5935

Chen, J.J., Jamialahmadi, M. and Li, S.M. (1989) Effect of liquid depth on circulation in bubble columns: a visual study, *Chem. Eng. Res. Des., 67*, pp.203-207

Deen, N.G. and Hjertager, B.H. (1999) Multiphase Particle Image Velocimetry Measurements in an Aerated Stirred Tank, presented at Annual Meeting AIChE, Dallas USA

Deen, N.G., Hjertager, B.H. and Solberg, T. (2000) Comparison of PIV and LDA Measurement Methods Applied to the Gas-Liquid Flow in a Bubble Column, 10th Intl. Symp. on Applications of Laser Techniques to Fluid Mechanics, Lisbon, Portugal

Delnoij, E., Lammers, F.A., Kuipers, J.A.M. and van Swaaij, W.P.M. (1997) Dynamic simulation of dispersed gas-liquid two-phase flow using a discrete bubble model, *Chem. Eng. Sci., 52*, pp.1429-1458

Eigenberger, G. and Sokolichin, A. (1997) Modellierung und effiziente numerische Simulation von Gas-Flüssigkeits-Reaktoren mit Blasenströmungen nach dem Euler-Euler-Konzept, DFG-Report, http://pcvt12.icvt.uni-stuttgart.de/alex/bericht_97h/bericht_97h.html

Friberg, P.C. (1998) Three-dimensional modelling and simulations of gas-liquid flow processes in bioreactors, PhD thesis Norwegian University of Science and Technology, Porsgrunn, Norway

Hjertager, B.H. (1998) Computational Fluid Dynamics (CFD) analysis of multiphase chemical reactors, *Trends in Chem. Eng., 4*, pp.45-92

Jakobsen, H.A. Sannæs, B.H., Grecskott, S. and Svendsen, H.F. (1997) Modeling of vertical bubble-driven flows, *Ind. Chem. Res., 36*, pp.4052-4074

Mudde, R.F. and Simonin, O. (1999) Two- and three-dimensional simulations of a bubble plume using a two-fluid model, *Chem. Eng. Sci., 54*, pp.5061-5069

Pfleger, D., Gomes, S., Gilbert, N. and Wagner, H.G. (1999) Hydrodynamic simulations of laboratory scale bubble columns fundamental studies of the Eulerian-Eulerian modelling approach, *Chem. Eng. Sci., 54*, pp.5091-5099

Sato, Y. and Sekoguchi, K. (1975) Liquid velocity distribution in two-phase bubble flow, *Int. J. Multiphase Flow, 2*, pp.79

Sokolichin, A. and Eigenberger, G. (1994) Gas-liquid flow in bubble columns and loop reactors: part I. Detailed modelling and numerical simulation, *Chem. Eng. Sci., 49*, pp.5735-5746

Sokolichin, A. and Eigenberger, G. (1999) Applicability of the standard k-ε turbulence model to the dynamic simulation of bubble columns: Part I. Detailed numerical simulations, *Chem. Eng. Sci., 54*, pp.2273-2284

Sokolichin, A., Eigenberger, G., Lapin, A. and Lübbert, A. (1997) Dynamic numerical simulations of gas-liquid two-phase flows, Euler/Euler versus Euler/Lagrange, *Chem. Eng. Sci., 52*, pp.611-626

Tomiyama, A. (1998) Struggle with computational bubble dynamics, 3rd Int. Conf. On Multiphase Flow, ICMF'98, Lyon, France